PROCEEDINGS OF SPIE

SPIEDigitalLibrary.org/conference-proceedings-of-spie

Performance overview of the Euclid infrared focal plane detector subsystems

A. Waczynski, R. Barbier, S. Cagiano, J. Chen, S. Cheung, et al.

A. Waczynski, R. Barbier, S. Cagiano, J. Chen, S. Cheung, H. Cho, A. Cillis, J-C. Clémens, O. Dawson, G. Delo, M. Farris, A. Feizi, R. Foltz, M. Hickey, W. Holmes, T. Hwang, U. Israelsson, M. Jhabvala, D. Kahle, Em. Kan, Er. Kan, M. Loose, G. Lotkin, L. Miko, L. Nguyen, E. Piquette, T. Powers, S. Pravdo, A. Runkle, M. Seiffert, P. Strada, C. Tucker, K. Turck, F. Wang, C. Weber, J. Williams, "Performance overview of the Euclid infrared focal plane detector subsystems," Proc. SPIE 9915, High Energy, Optical, and Infrared Detectors for Astronomy VII, 991511 (29 July 2016); doi: 10.1117/12.2231641

SPIE.

Event: SPIE Astronomical Telescopes + Instrumentation, 2016, Edinburgh, United Kingdom

Performance Overview of the Euclid Infrared Focal Plane Detector Subsystems

A. Waczynski[1], R. Barbier[2], S. Cagiano[1], J. Chen[3], S. Cheung[3], H. Cho[4], A. Cillis[5], J-C. Clemens[6], O. Dawson[4], G. Delo[7], M. Farris[8], A. Feizi[9], R. Foltz[1], M. Hickey[1], W. Holmes[4], T. Hwang[3], U. Israellson[4], M. Jhabvala[1], D. Kahle[1], Em. Kan[1], Er. Kan[1], M. Loose[10], G. Lotkin[1], L. Miko[1], L. Nguyen[1], E. Piquette[8], T. Powers[3], S. Pravdo[4], A. Runkle[4], M. Seiffert[4], P. Strada[11], C. Tucker[2], K. Turck[5], F. Wang[3], C. Weber[3], J. Williams[7]

[1]NASA Goddard Space Flight Center, 8800 Greenbelt Rd., Greenbelt, MD 20771 USA
[2]Institut de Physique Nucléaire de Lyon, 4 Rue Enrico Fermi, Villeurbanne, 69622 FR
[3]Arctic Slope Regional Corporation, 7000 Muirkirk Meadows Dr., Beltsville, MD 20705 USA
[4]Jet Propulsion Laboratory, 4800 Oak Grove Dr., Pasadena, CA 91109 USA
[5]University of Maryland Baltimore County, 1000 Hilltop Cir., Baltimore, MD USA 21250 USA
[6]CNRS, Centre de Physique des Particules de Marseille, 163 Ave. de Luminy, Marseille 13009 FR
[7]Global Science and Technology, 7855 Walker Dr., Greenbelt, MD 20770 USA
[8]Teledyne Imaging Sensors, 1049 Camino Dos Rios, Thousand Oaks, CA 91360 USA
[9]AK Aerospace Technology Corporation, 4300 B St., Anchorage, AK 99503 USA
[10]Markury Scientific Inc, 518 Oakhampton St., Thousand Oaks, CA 91361 USA
[11]European Space Research and Technology Centre, Keplerlaan 1, AZ Noordwijk 2201 NL

ABSTRACT

In support of the European Space Agency (ESA) Euclid mission, NASA is responsible for the evaluation of the H2RG mercury cadmium telluride (MCT) detectors and electronics assemblies fabricated by Teledyne Imaging Systems. The detector evaluation is performed in the Detector Characterization Laboratory (DCL) at the NASA Goddard Space Flight Center (GSFC) in close collaboration with engineers and scientists from the Jet Propulsion Laboratory (JPL) and the Euclid project. The Euclid Near-Infrared Spectrometer and Imaging Photometer (NISP) will perform large-area optical and spectroscopic sky surveys in the 0.9-2.02 μm infrared (IR) region. The NISP instrument will contain sixteen detector arrays each coupled to a Teledyne SIDECAR application specific integrated circuit (ASIC). The focal plane will operate at 100K and the SIDECAR ASIC will be in close proximity operating at a slightly higher temperature of 137K. This paper will describe the test configuration, performance tests and results of the latest engineering run, also known as Pilot Run 3 (PR3), consisting of four H2RG detectors operating simultaneously. Performance data will be presented on; noise, spectral quantum efficiency, dark current, persistence, pixel yield, pixel to pixel uniformity, linearity, inter pixel crosstalk, full well and dynamic range, power dissipation, thermal response and unit cell input sensitivity.

Keywords: Euclid, mercury cadmium telluride detectors, infrared focal planes, IR detector arrays

1. INTRODUCTION

Development of detector technology for Euclid NISP instrument started with the ESA program of technology development (called NRE phase) at Teledyne Imaging Systems (TIS) in 2012. Its primary goal was to demonstrate that the Euclid IR detectors will the meet requirements with a reasonable yield. Since ESA decided to procure a system composed of an IR array and Sidecar ASIC cold electronics it was equally important to establish a fabrication process and flight qualify the whole system composed of the H2RG detector Sensor Chip Assembly (SCA), Sidecar Sensor Chip Electronics (SCE) module and the connecting Cryo Flex Cable (CFC) shown below in figure 1. All three together are known as the Sensor Chip Subsystem (SCS) NRE detectors have been manufactured and tested by TIS and then some of them were retested at DCL. At this point the DCL has tested 8 of engineering SCAs as single detectors and in the SCS

High Energy, Optical, and Infrared Detectors for Astronomy VII, edited by Andrew D. Holland, James Beletic,
Proc. of SPIE Vol. 9915, 991511 · © 2016 SPIE · CCC code: 0277-786X/16/$18 · doi: 10.1117/12.2231641

configuration with an engineering SCE and CFC. This paper reports on DCL testing methods and results. At the present time, DCL is moving from testing engineering devices to the flight phase. For the Euclid Flight instrument a total of 20 flight SCS modules, including 4 spares, need to be tested, flight qualified and delivered to ESA. The factory delivery schedule of flight components leaves a limited time window for SCS acceptance testing. The ongoing testing of engineering modules is used as a pathfinder for flight testing by verifying the facility, test procedures, data analysis, reporting and test personnel.

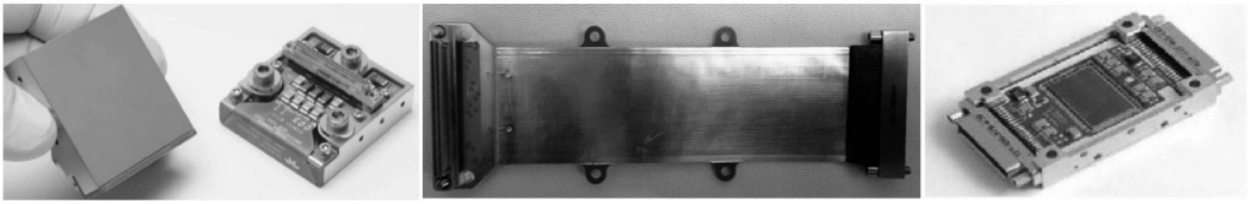

Figure 1. The SCA, CFC and SCE components comprising the SCS unit.

2. EUCLID DCL TEST FACILITY

The DCL has supported multiple flight programs, developing extensive test capabilities including facilities, instrumentation, and testing methods. The Euclid SCS performance specification, the number of modules, and their tight delivery schedule required an upgrade to some of the existing test setups and also the commissioning of new ones. The Euclid testing is composed of three phases: testing of individual components, selection and integration of flight candidates into SCS modules, and the final acceptance testing of SCS modules. The detector operates at a cryogenic temperature of 100K but the SCE operates at 125K and each of the three components will be tested in individual setups at various cryogenic temperatures to explore its flight worthiness and evaluate the relevant parameters under the operating conditions. Up to five of SCA detectors can be tested at the same time using a single detector setup and a four detector setup. Simultaneous testing of multiple detectors in the same setup has an additional benefit of precise comparison of detector properties on relative scale. Similar to the SCA, a single test setup supports parallel testing of four SCE with the option to extend it to 12 units. The test setup emulates electrical signals to the SCE input enabling measurements of noise, differential nonlinearities, and other electrical parameters under Euclid operating conditions.
The CFC test setup supports parallel testing of eight CFC at cryogenic temperatures. As the temperature is varying from room to 80K the cable trace resistance is continuously monitored and recorded. The resistance profile is compared with the expectation and anomalous cables are rejected.

The SCS acceptance testing is supported by the primary Euclid SCS test setup which accepts four SCS modules at a time. The primary SCS setup is based on a large cryostat, shown below in figure 2 with internal optics ensuring very low thermionic background. The cryostat is equipped with cold shutters and can be configured for dark or for photometric measurements with monochromatic illumination covering the Euclid spectral range with adjustable spectral resolution of a few to tens of nanometers. Monochromatic irradiation is projected on the detector plane through an internal integrating sphere with illumination uniformity better than 0.5%. The detector can be also illuminated with Fe55 photons, controlled by an internal shutter. The SCA signal is digitized by SCE and is send out through LVDS transmission line to a controller made by Marcury Scientific. The data stream from multiple outputs is formatted by controller and sent to the host computer through a Camera Link interface. The data is captured by a Matrox frame grabber, formatted, and stored to hard drive. The Euclid test facilities are class 100 clean rooms qualified for flight work against NASA standards.

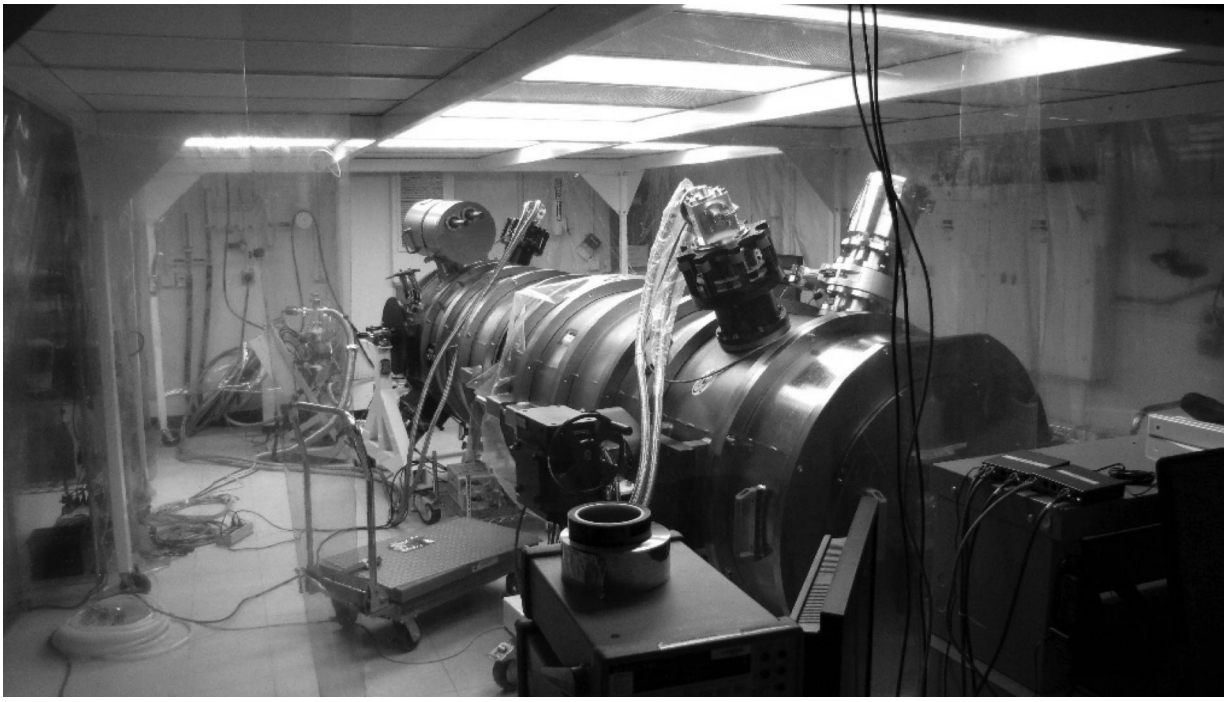

Figure 2. The DCL large test dewar.

3. EUCLID TEST REQUIREMENTS

The Euclid NISP instrument operates in spectroscopy and photometry modes. Consequently, Euclid SCS requirements are specified for the corresponding modes and need to be verified under corresponding modes of data acquisition. Key electro-optical performance requirements are listed in **Table 1**. The requirements stipulate that an acceptable SCS has more than 95% of pixels meeting the specification for quantum efficiency (QE), spectroscopy noise, photometry noise, and linearity. Pixels meeting these four requirements are referred to as science pixels. Almost all the performance parameters are specified on a per pixel basis. Verification of acceptance parameters has to be performed for each pixel with reasonable accuracy. Ground based testing may be used for instrument calibration. NISP is expected to detect 24 magnitude sources with 95% of observations focused on low brightness objects. Since NISP is targeting 1% measurement accuracy, corresponding test accuracies are expected. Test accuracy is one of the most difficult aspects of Euclid SCS testing, challenging methodology and schedule. Acquisition of low intensity objects requires a high signal to noise ratio consequently making quantum efficiency and noise key performance parameters. Since the NISP instrument operates in two different modes the noise specification is derived independently for each of them, accounting for the data sampling scheme and exposure time. As with most of acceptance requirements, noise has to be verified for each science pixel.

For both modes, the NISP data acquisition is based on a Sample-Up-The-Ramp (SUTR) sampling scheme. In the spectroscopy mode a single reset frame is followed by 15 groups of 16 frames, separated by 13 ‘drop’ frames evenly spaced over a 560 second exposure time. In the photometry mode a reset frame is followed by 3 groups of 16 frames, separated by 3 ‘drop’ frames. In both cases the pixel rate is 100 kHz, with 32 readout channels, yielding a frame time of 1.4 seconds.

Table 1 Summary of SCS requirements

Name	Value	Comment
Spectroscopy Noise	< 13e for 95% of pixels in 560s ramp of 15group of 16frames	13 drop frames
Photometry Noise	< 9e for 95% of pixels in 60s ramp of 3 group of 16 frames	4 drop frames
Quantum Efficiency	> 74% for 95% of pixels	
Non-Linearity	< 5% for 95% of pixels between 6ke and 60ke	
Spectral range	$935 < \lambda < 2020$ nm	
Persistence	< 0.05e/s for 95% of pixels at 60ke accumulation < 0.15e/s for 95% of pixels at 400ke accumulation < 0.18e/s for 95% of pixels at 100ke accumulation	
Median Dark Current	< 0.07e/s at 100K	
IPC Crosstalk	< 2% over nearest neighbor pixels	
Channel Crosstalk	< 0.3% output to output (32 outputs)	
Dynamic Range	> 65ke for 98% of science pixels	
SCS Thermal Sensitivity	The SCS performance shall be met over ±10mK variation over 560s of SCA temperature and ±100mK variation of SCE temperature	

4. TESTING APPROACH

A. Noise

Spectroscopy Noise is defined as the uncertainty of the integration slope for either of the two modes. In order to measure pixel noise with an accuracy of approximately 10%, the test is composed of 100 exposures of 450 frames with continuous sampling. The resulting data set can be analyzed for spectroscopy or photometry noise with the appropriate groupings of frames.

B. Dark Current

Dark current, derived from the noise data, is the average slope for a given pixel in the set of 100 exposures. However, a relatively short exposure time combined with the read noise and system instability leads to significant error in the per pixel dark current measurement. In a separate test, dark current is measured again by acquiring a sequence of 2-hour exposures. A longer exposure time results in a significant reduction of the measurement error.

C. Quantum Efficiency (QE)

A substitution method is used to evaluate the detector QE. A National Institute of Standards and Technology (NIST) traceable, calibrated photodiode is placed in the detector focal plane to calibrate the radiometric flux. The response of detector under the test is compared with the photodiode signal to estimate the detector QE. Measurements are performed over the wavelength range of 850nm to 2.5µm in steps of 50nm, covering the science spectral range of 900nm to 2.02µm and detector cutoff of 2.3µm. The QE raw data is also used to evaluate the detector non-uniformity and QE spectral gradients.

D. Linearity

The Euclid mission requires that the pixel response linearity be verified within a 60ke signal range. Linearity data is collected as a set of 10 exposures of 450 frames with the illumination adjusted to exceed 60ke accumulation but avoid pixel saturation. The integration ramp of each pixel is evaluated by fitting a second order polynomial and verifying that the residuals remains below 5% over a signal range of 6ke to 60ke.

E Persistence

The persistence is the residual signal that remains once the pixel has been reset. The Persistence is measured by exposing the detector for 560 seconds to a flux level adjusted to reach accumulation of required level of charge. A sequence of 560s dark exposures is collected over a period of approximately 7 hours. Persistence is measured for the accumulation of 60ke, 400ke and 1000ke, to assess the detector response for signals within the SCS dynamic range and signals that saturate the detector full well.

F. Crosstalk

The crosstalk caused by Inter Pixel Capacitance (IPC) and channel-to-channel crosstalk is evaluated. IPC crosstalk is measured using a single pixel reset method and is collaborated with x-ray Fe^{55} source images. Channel-to channel crosstalk is measured using a special acquisition mode, which at a given time injects signal into a single channel and examines all the remaining channels. This test is performed for unsaturated and saturated levels of injected signal.

G. Gain

SCS conversion gain is measured using a photon transfer method. Low-level illumination is used to avoid response nonlinearity. Multiple exposures are collected to estimate the measurement error. Additionally, the per channel electrical gain of the readout and cold electronics (SCE) is measured by collecting data with the SCA reset switch turned on. This data is used for image correction.

H. SCS Thermal Sensitivity

SCS thermal sensitivity is computed from the baseline images acquired at the SCA temperatures of 90K, 100K and 110K. During this test the SCE is maintained at a constant temperature of 125K. A similar test is performed for the SCE by changing its temperature to 125K and 145K while maintaining the SCA at 100K. It has been shown that in the Euclid SCS configuration the SCE temperature sensitivity is very low compared to that of SCA.

5. TEST RESULTS

While the primary reason for component testing is to select flight candidates and reject faulty units, SCS testing will generate data representing the final module configuration and these test results may be used during instrument calibration and modeling. In the following we discuss selected SCS test results from most recent testing campaign called Pilot Run 3 (PR3). This run included four SCS modules, three of which were Grade 1 (Flight-worthy) NRE modules

A. Noise

The Euclid SCS specification has separate noise figures for spectroscopy and for photometry, shown in **Table 1**. Noise is specified as a limit for 95% of pixels – more specifically, it is required that 95% of pixels simultaneously meet the required noise, QE, and linearity specs. Spectroscopy noise is measured as the uncertainty of the slope derived from a SUTR exposure composed of 15 groups of 16 frames uniformly distributed over integration time of 560 seconds. For a given test we collect approximately 100 exposures to ensure an accuracy better than 10% for the per pixel noise measurement. Similarly, photometry noise specification requires that a limit of 9e RMS be met by at least 95% of pixels in a 60 second exposure with 3 groups of 16 frames.

Noise is measured by acquiring exposures of 450 frames, continuous sampling over 635 seconds. Both, spectroscopy and photometry noise are computed from a single data set by correspondingly reformatting the data. This approach minimizes data acquisition time for the price of slightly larger data set. The NRE detectors tested at DCL have met the noise requirements. **Figure 3** shows the noise histograms and images for PR3 detectors and Table **2** shows the median noise values and the number of pixels below threshold. Since the median values are much lower than the required noise threshold, a 10% accuracy of noise per pixel determination translates into significantly better accuracy when determining the number of pixels meeting the requirements. It should be noted that Euclid SCS noise is significantly higher than the corresponding SCA noise due to the SCE noise component. The noise difference between SCS and corresponding SCA can be as high as 20%.

Table 2 Spectroscopy and photometry noise figures

	Spectroscopy		Photometry	
	Median Noise [e]	% of pixels passing	Median Noise [e]	% of pixels passing
17243	5.4	97.9	5.2	98.7
17192	5.3	95.8	4.6	97.3
17178	5.4	97.2	5.2	97.9
17246	5.8	98.0	5.8	98.4

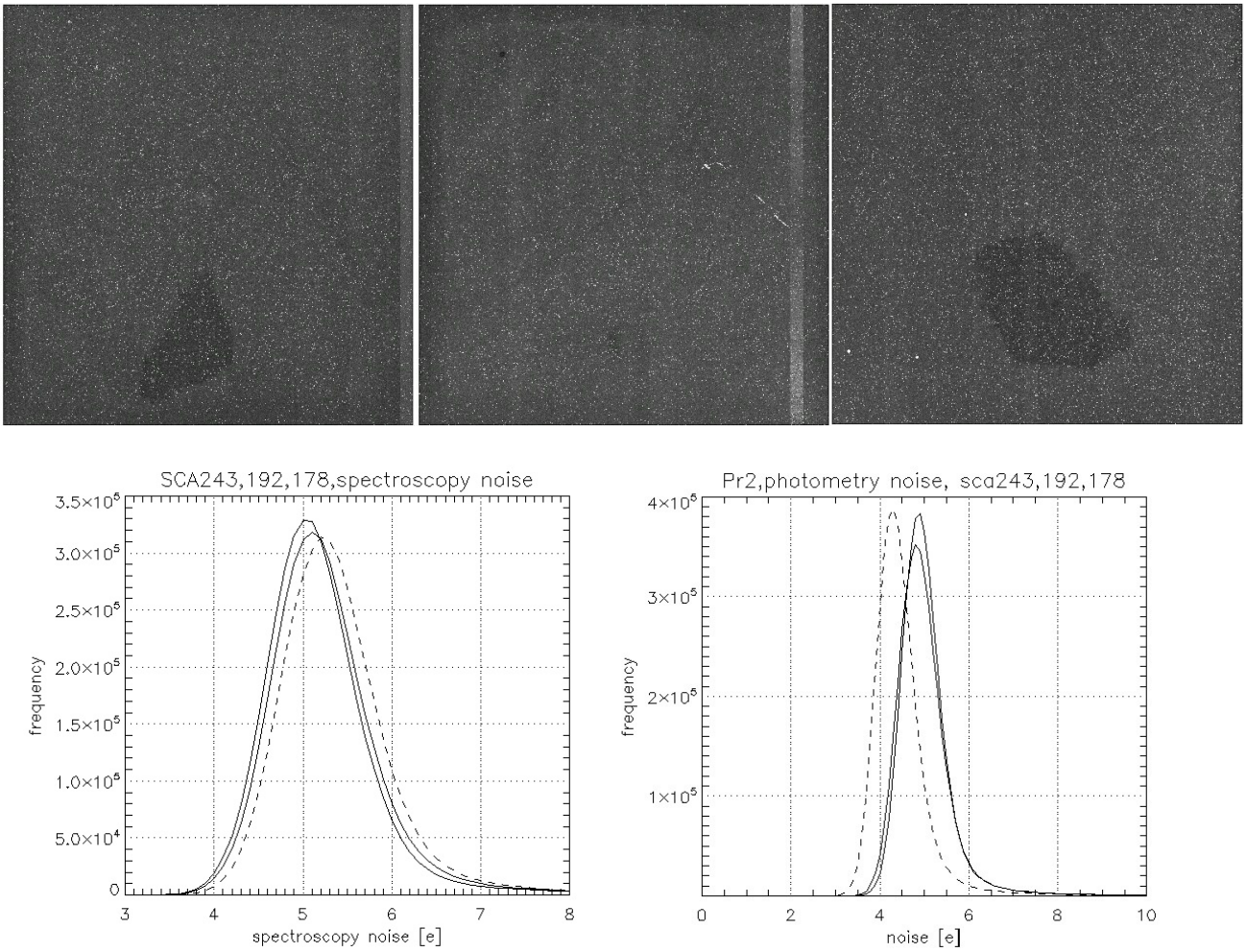

Figure 3 Spectroscopy and photometry noise of the 3 grade 1 NRE detectors. Top images show spatial uniformity of the spectroscopy noise, lower plots show histograms of spectroscopy and photometry noise.

B. Dark Current

NRE detectors meet the Euclid NISP SCS dark specification by a large margin. At 100K, the dark current of 2.3μm cutoff HgCdTe from TIS is typically below 0.02e/s. Accurate determination of dark current per pixel is challenging because of its low value and limited understanding of low level SCS system instability. Dark current can be determined from the noise data set, however better accuracy can be obtained from additional testing using long, 2-hour exposures. **Figure 4** shows the results obtained during PR3 run.

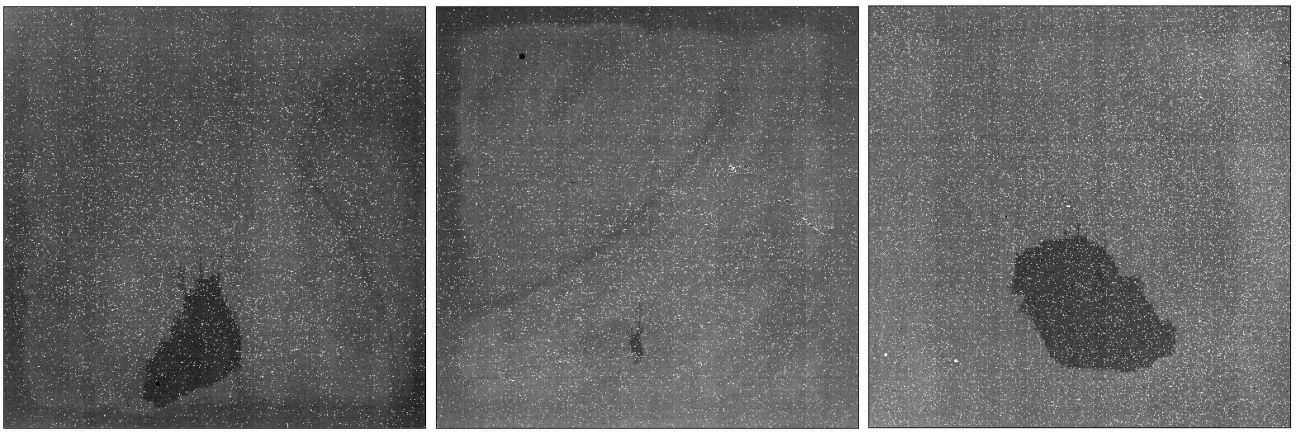

Figure 4a. Dark current images obtained from 2h dark exposure. From left to right: SCA17243, 17192, 17178

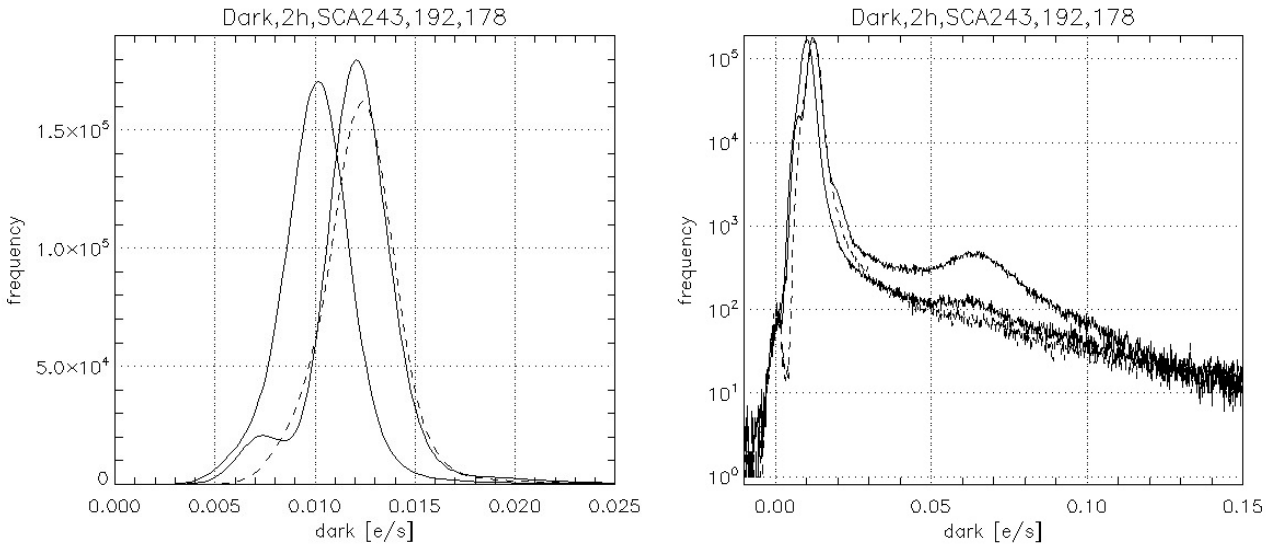

Figure 4b. Dark current histograms for 3 grade 1 NRE detectors, left - linear scale, right - logarithmic scale

C. Quantum Efficiency

The Euclid detectors are backside thinned with an antireflective (AR) coating matched to the science-determined spectral range of 900nm to 2.02µm. The QE requirements are specified for each wavelength as shown in **Figure 5**. Verification of the requirement is performed for the science spectral range with a resolution of 50nm and is extended to 2.4µm to evaluate the detector cutoff wavelength at 2.3um. The QE measurement is based on a substitution method; first, a NIST calibrated reference detector is placed in detector plane to calibrate radiometric flux at each measured wavelength, then, the detectors are placed in the same plane and their response to spectral flux is compared to that of the reference detector. Most of the tested NRE detectors show excellent QE, significantly exceeding the requirements. With exception of one, they have good cosmetics and show good uniformity of response at all wavelengths – typically the per pixel non-uniformity stays below 3%. **Figure 5** shows the QE measured for the PR3 detectors. We estimate that QE is measured with 5% error due to the inaccuracy of the gain determination and other systematic and random error sources.

As a part of our error analysis we have performed a study of quantum yield by measuring photon transfer gain as a function of wavelength. We have not observed any spectral dependence in the gain determination and concluded that quantum yield is not a significant factor in the QE determination for the Euclid spectral range.

Figure 6a and 6b show excellent uniformity of photo response with a ratio of standard deviation to mean in range of single percent. One of the three detectors has higher pixel to pixel non-uniformity although still well within Euclid specification.

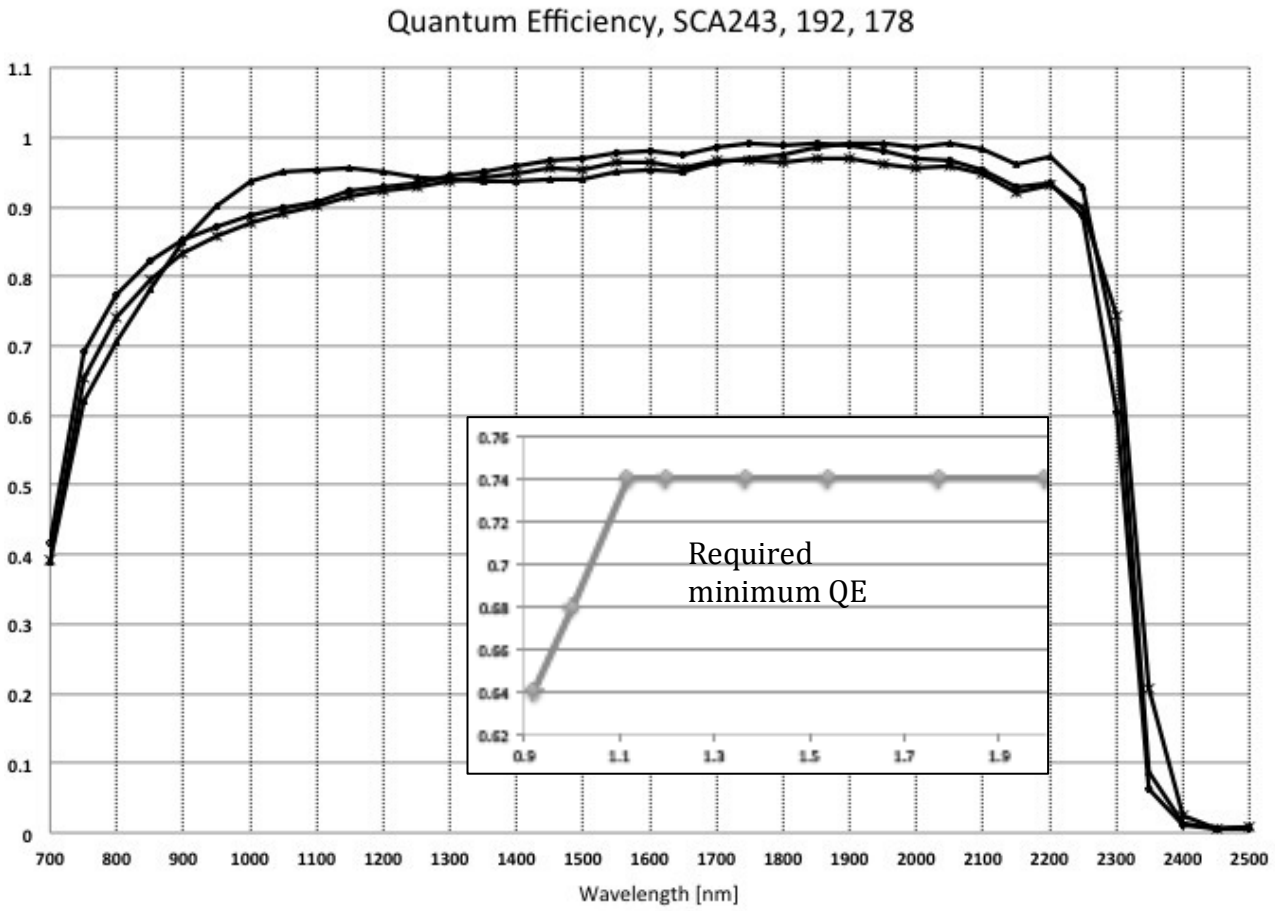

Figure 5 Plot of quantum efficiency versus wavelength as measured for grade 1 NRE detectors. Insert shows Euclid requirements.

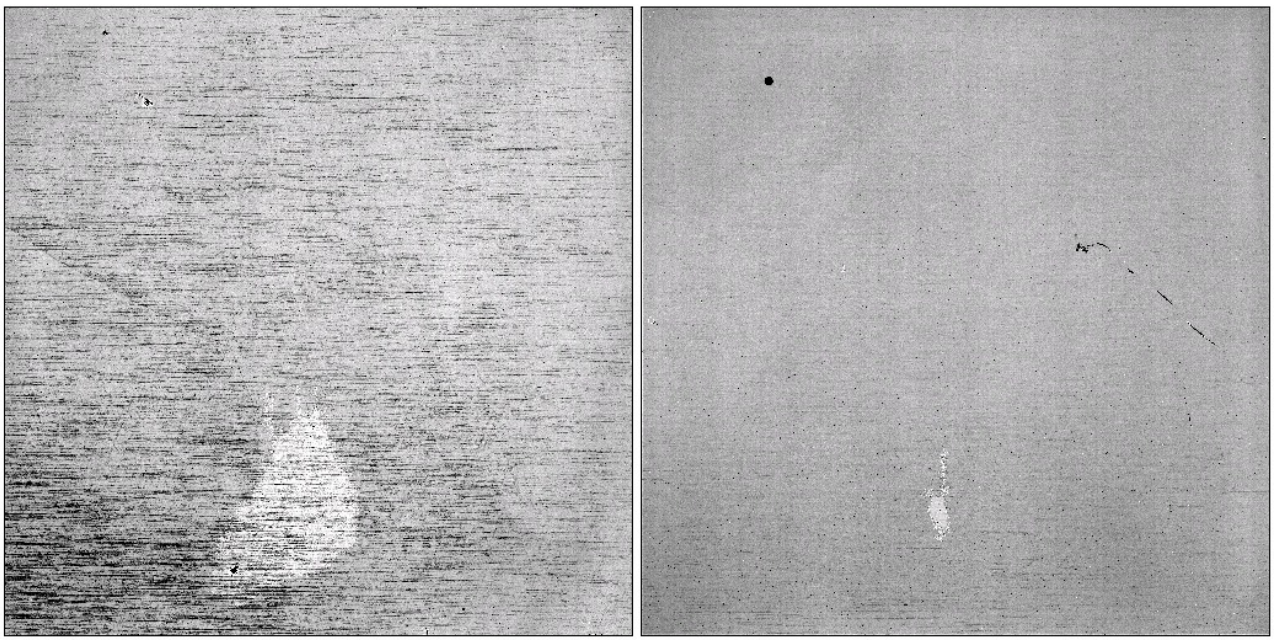

Figure 6a Flat fields at 1400nm, SCA17243 - left, SCA17192 - right

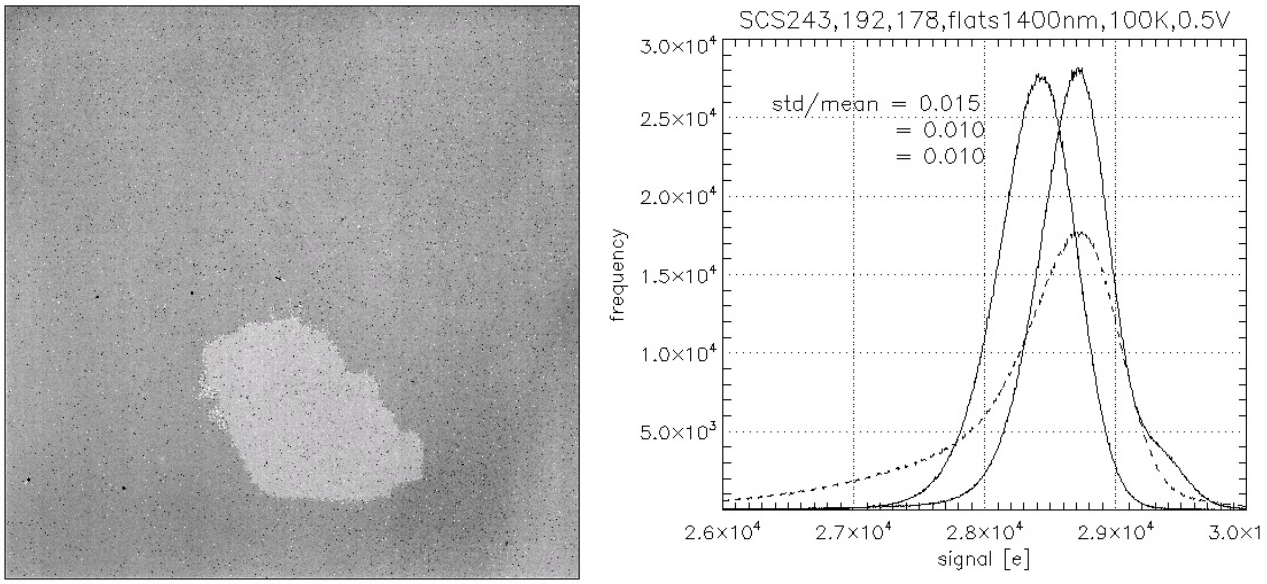

Figure 6b. On left, flat field of SCA17178, on right flat field histograms. Ratio of standard deviation to signal mean includes all possible non-uniformity causes, between them spatial non-uniformity of gain.

D. Persistence

Many detectors suffer from a persistence (or latency) phenomenon that becomes one of the most annoying problems for astronomy applications requiring high sensitivity measurements of very weak signals. Unfortunately, Euclid IR detectors are not free of this effect. The NRE detectors have shown a variety of behaviors where some of units had very low persistence, barely detectable, while others had persistence so large that it was difficult to assess other performance parameters like dark and noise. The NISP team expended a significant effort to assess impact of persistence on Euclid science and in support, the test labs are requested to characterize the NRE detectors for persistence effects. **Figure 7** shows the results of persistence versus illumination (or more accurately versus accumulated signal) for SCA17186 and for three Grade 1 detectors. This behavior is typical for Euclid detectors we have tested, but there are still significant differences between units as their response varies by more than an order of magnitude. Experimental results led to the

formulation of the present NISP persistence specification with limits specified for the three levels of illumination resulting in accumulation of 60ke, 400ke and 1000ke over a typical exposure time of 560 seconds. Since the NISP observing strategy is to exclude pixels exposed to high flux from the next observations, the specification requires that persistence should be measured 5 hours after illumination. Consequently, the test has to be performed over more than 5 hours for a single point persistence determination. The persistence specification needs to be verified on per pixel bases. At the illumination level equivalent to 60ke, persistence needs to be lower than 0.05e/s for at least 95% of pixels. Additionally, the persistence determination requires a subtraction of dark current to remove hot pixels and the dark current pedestal. It follows then, that in order to obtain 10% accuracy of per pixel persistence measurement, one must be able to measure per pixel dark with accuracy better than 0.003e/s. Theoretically, such accuracy of dark is possible if we average 100 exposures of noise data. However, experiments indicate that there are other sources of noise that increase the measurement error above its theoretical expectation. Better accuracy can be obtained when measuring dark current with longer exposures, as shown in **Figure 9**.

It is even more challenging to obtain the accuracy needed in the persistence data. Persistence is measured as the signal in a sequence of dark, Euclid like, 560 second exposures following a 560 second illumination – see **figure 8**. Persistence decay is a nonlinear process well described by a power law, as shown in **Figures 8 and 9**. It follows that in a single experiment, the per pixel persistence measurement accuracy is in the range of 0.03e/s, clearly this is not adequate to determine if a given pixels falls in or out of 0.05e/s spec. Averaging multiple persistence runs to reduce measurement error is not practical considering that the total time required to make a single measurement exceeds 8 hours. Instead, we have been exploring the use of a power law fit on the time sequence of decay to reduce the error. **Figures 10** show preliminary results. Compared to the persistence estimation based on single exposure collected 5hr after illumination, the power fit approach significantly reduces measurement errors making it possible to verify the challenging specification with reasonable accuracy. **Figures 8 and 9** show the decay of the median persistence of the four PR3 detectors, the numerical data is shown in **Table 3**. The PR3 detectors comfortably meet the persistence specification, although the median persistence for a particular illumination level does vary significantly within the group. Unfortunately, some of the NRE detectors have persistence large enough to fail the persistence specification while passing all other requirements. In addition to variation between detectors, persistence varies significantly between the pixels of the same detector array. Non-uniformity is most prominent in the initial exposures after illumination. The persistence variation between pixels is much smaller at the 5 hour point.

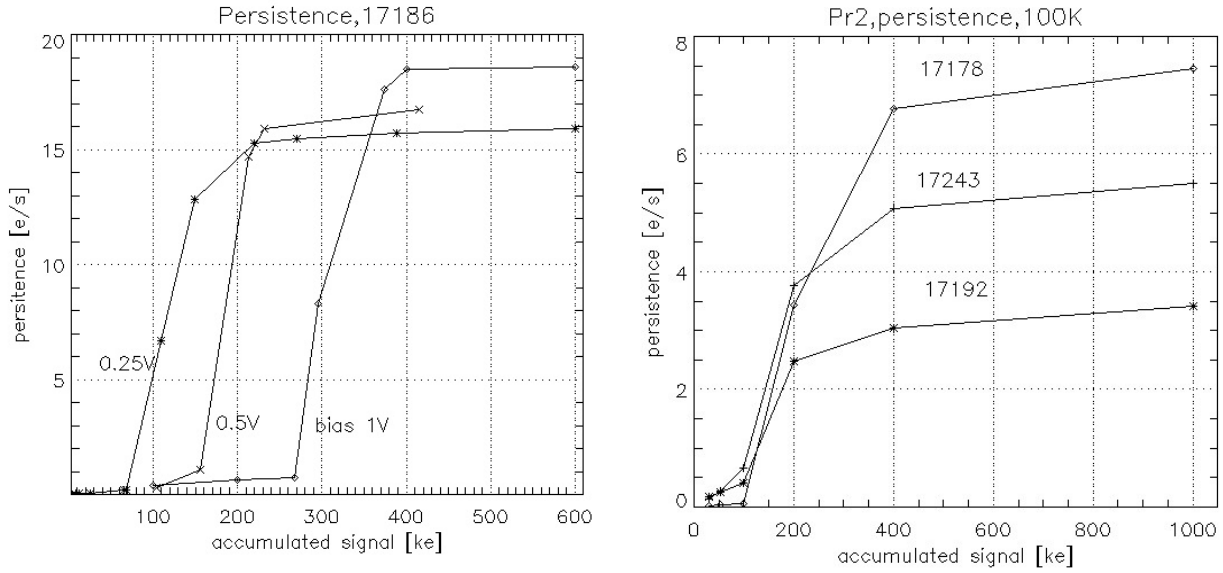

Figure 7. Persistence versus accumulated charge during 560s illumination. Each point represents rate of dark signal during first 560s after illumination

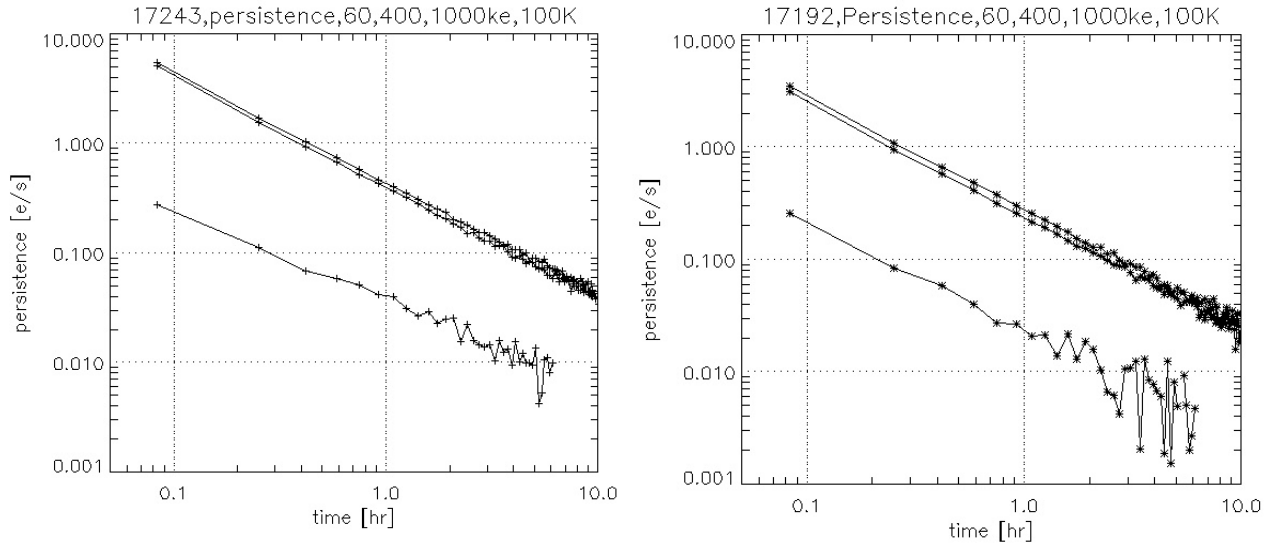

Figure 8. Persistence decay versus time after different illumination exposure. Each point represents averaged dark signal in 560s exposure. Lowest trace corresponds to accumulation of 60ke; upper traces correspond to 400ke and 1000ke.

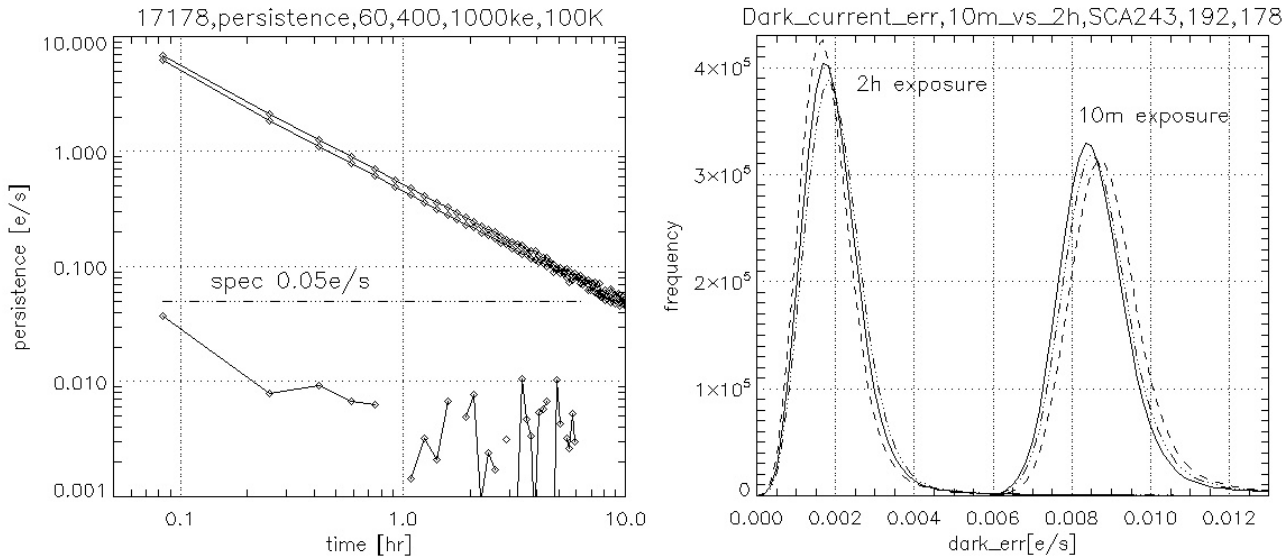

Figure 9. Left: Persistence decay versus time after different illumination exposure. Each point represents averaged dark signal in 560s exposure. Lowest trace corresponds to accumulation of 60ke; upper traces correspond to 400ke and 1000ke. Right: comparison error of the dark current measurement for different exposure times; 560s versus 2 hours. Longer exposure time yields a higher precision of measurement for a given test duration.

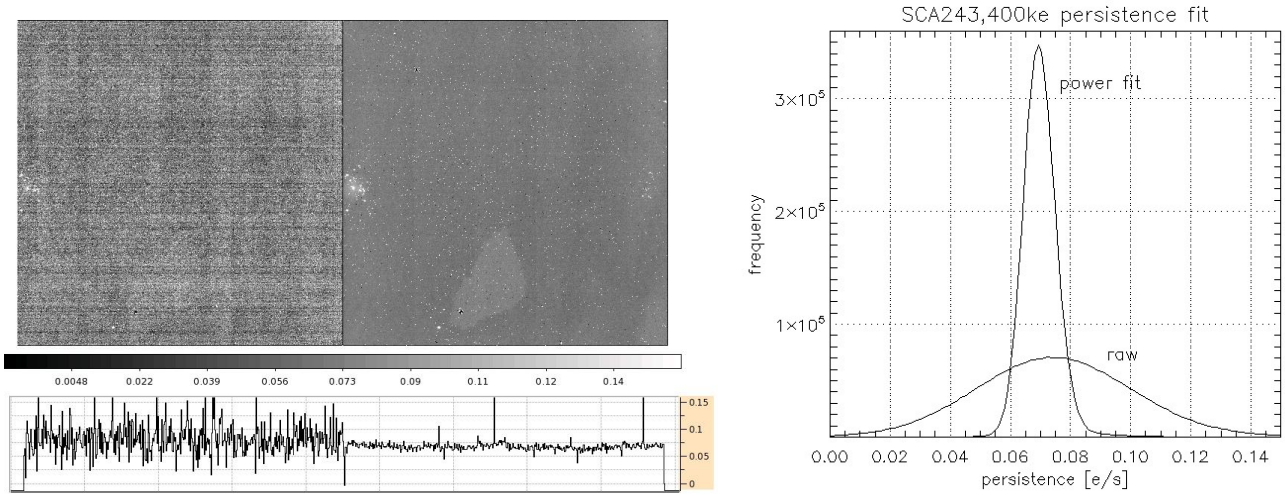

Figure 10. Accuracy of persistence measurement can be improved by application of a power fit. Left: Comparison of raw and fit persistence images after 5 hours from illumination. Right: Corresponding histograms, five hours after illumination persistence dispersion is dominated by the random error.

Table 3 Persistence of four Euclid detectors

	60ke		400ke		1000ke	
	Median [e/s]	% pix pass	Median [e/s]	% pix pass	Median [e/s]	% pix pass
17243	0.008	99.3	0.08	99.7	0.09	99.7
17192	0.006	99.8	0.05	99.9	0.06	99.9
17178	0.001	98.6	0.1	98.1	0.11	98.7
17246	0.003	99.5	0.16	31.2	0.18	52.2

E. Crosstalk

The NISP specification calls for the verification of pixel-to-pixel crosstalk due to parasitic inter-pixel capacitance (IPC) and inter-channel crosstalk resulting from the wiring and readout electronics. IPC crosstalk easily passes the specification with a large margin, typically staying below 0.8% while the requirement is for less than 2%. Similarly, the channel-to-channel crosstalk requirement of 0.3% is easily met in the SCS configuration with a typical value of less than 0.01%.

The IPC crosstalk is measured by the single pixel reset method–an 8x8 grid of pixels is selectively reset to a new reset value causing a reflow of charge from the reset pixel to its neighbors through the parasitic network of inter-pixel capacitance. The IPC is reported as the median value of interrogated pixels, however, as shown in **Figure 11**, the tight spatial distribution implies that all pixels are likely to stay well below 2% requirement.

The inter-channel crosstalk is measured by injecting a signal into a given channel, resetting a selected group of pixels within the channel (using the H2RG window mode), and then monitoring the remaining channels for the crosstalk. This test is repeated for each channel, injecting signal on the image diagonal as shown in **Figure 12**. The level of injected signal is adjusted to get the crosstalk from unsaturated and saturated sources.

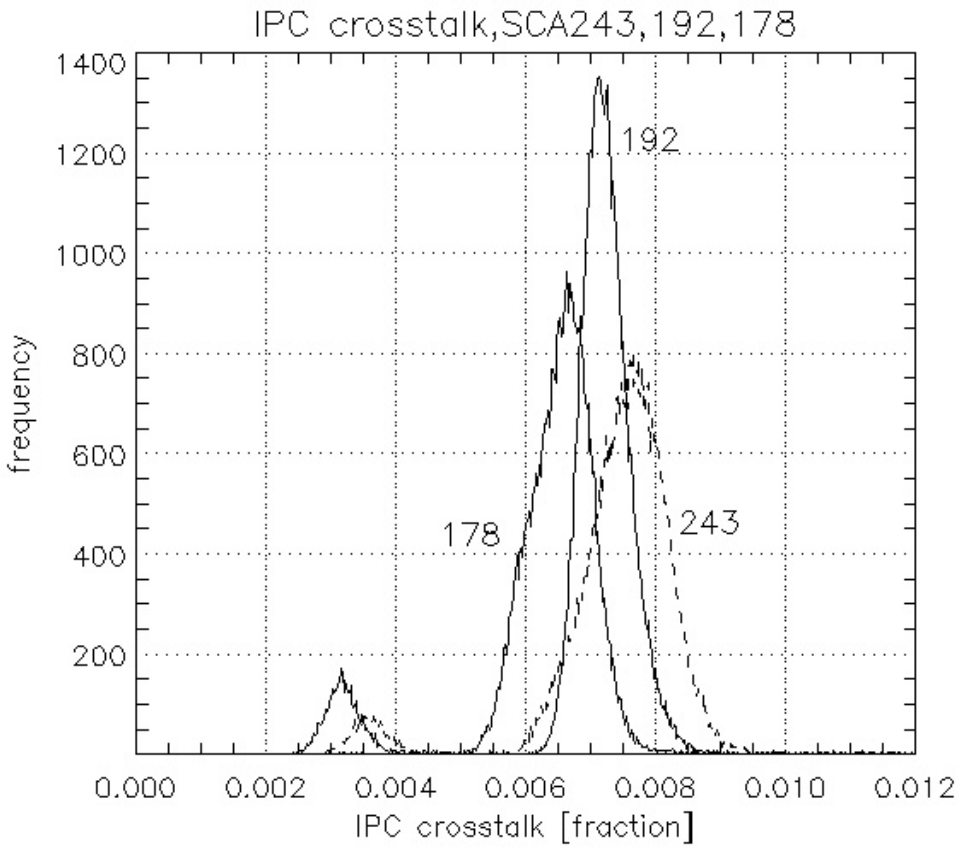

Figure 11. The IPC crosstalk histograms for three Grade 1 detectors. The width of the histograms is indicative of the spatial variability within a given detector. The ratio of the standard deviation to mean varies from 4% to 8%.

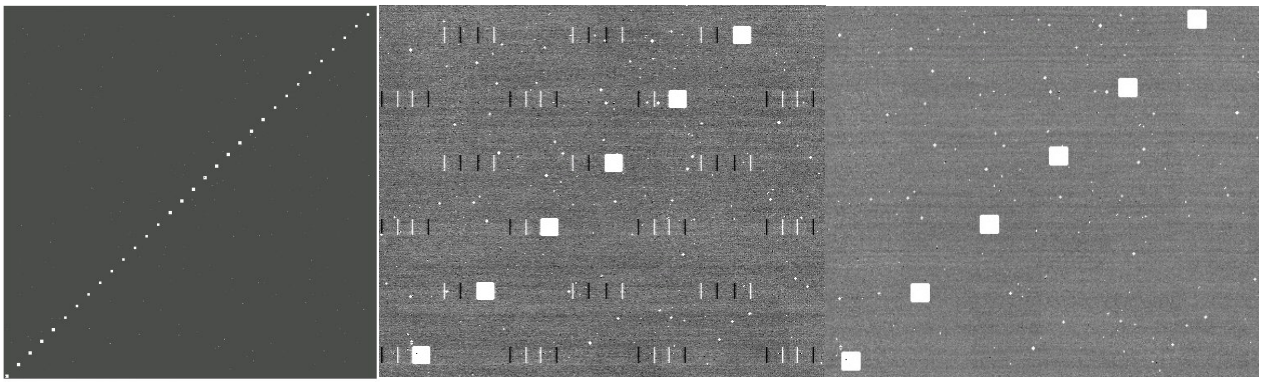

Figure 12. Images of crosstalk between readout channels. Left: the diagonal injection pattern; Center: shows the expanded sub-image with injection squares and resulting crosstalk in neighboring channels acquired in SCE differential mode; Right: the image is the same but in single ended input mode – note the significant difference of crosstalk magnitude between the two SCE input modes.

F. Linearity

The NISP science depends on the non-linearity correction that is reflected in formulation of the linearity requirement. The requirement states, that the deviation of the SCS response for each operable pixel, from the best polynomial

(quadratic) fit of the data obtained during an illuminated exposure, shall not exceed 5% throughout the range [6 Kphe- to 60 Kphe-]. We should note that the quadratic fit better approximates the detector response than a linear fit while higher order polynomials do not make any significant improvement. We measured the linearity by acquiring multiple exposures to fixed flux illumination covering a signal accumulation range from 0 to 65ke. Linearity analysis relies on the quadratic fit per pixel, performed over signals in the 6ke to 60ke range, which is then used to calculate the fit residuals normalized to the local fit value. **Figure 13** shows the distribution of maximum normalized fit residuals for the four PR# detectors. Note that in these IR detectors, the linearity of the response may depend on the previous history of the pixel illumination.

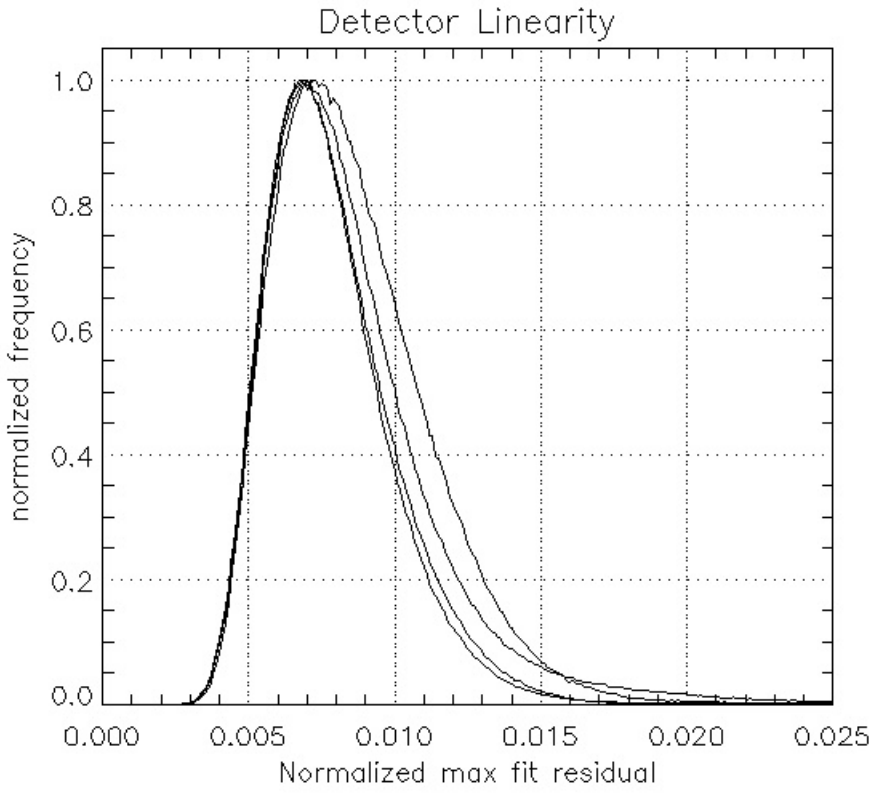

Figure 13. The histograms of the normalized maximum of pixel residual of the quadratic fit. A second order polynomial is fit to each pixel integration curve and the maximum deviation between the fit and the curve is normalized by the local fit value and plotted in the histogram. The histogram central value is much lower than the 5% linearity specification.

G. Dynamic Range and Full Well

In the SCS configuration the range of signal available to the user is determined by the effective gain and range of the analog to digital converter (ADC). The detector full well is set by its integrating capacitance and applied bias voltage. Since the bias voltage is a 'free parameter' it can be set high enough to ensure that the pixel full well exceeds the desired dynamic range. Presently, Euclid detectors use a nominal bias of 0.5V and their unit cell sensitivity is approximately 5μV/e yielding an average SCA full well of more than 100ke.This is significantly above the required 60ke for SCS, thus the full well is not a limiting factor in the derivation of the SCS useful range of operation or dynamic range. The primary factors in determining dynamic range are the detector pixel-to-pixel reset level variation, system gain, and the resolution and nonlinearity of the ADC converter. The pixel reset level sets the starting point for the signal integration and therefore needs to be positioned within the range of the ADC converter. The pixel-to pixel variation of the reset level may be as high as 25ke, effectively forcing the system design to use a lower gain in order to secure an additional 25ke of conversion range. An additional limitation comes from the nonlinearity of the ADC converters. At both extremes of the 16 bit range the SCE digital converters show significant nonlinearity, effectively removing an additional 5ke from the available range. In the initial SCS configuration the SCE gain was set to 18dB (or 8V/V) resulting in average system gain of ~0.8counts/e. As more detectors were tested it became apparent that this setting is marginal as some detectors were failing the specification due to a higher than average conversion gain. After studying the noise impact, the project team has recommended changing the gain to 15dB thus opening the dynamic range for higher conversion gain detectors.

H. Gain calibration

The SCS gain calibration consists of measuring the system gain [counts/electron], electrical gain [V/V] and multiplexer gain [V/V]. The system gain, derived from the photon transfer method of measurement is a critical parameter since it is used to calculate most of the other performance parameters. Electrical gain and multiplexer gain provide additional, but less critical, information mostly used for trend monitoring and diagnostics as well as for correction of the channel-to-channel gain non-uniformity.

The system gain is measured as a single parameter for a given SCS. It is desirable to measure the gain for each individual pixel with a 1% accuracy. Multiple attempts to make such measurements however have resulted in large errors. A large volume of data has to be collected to make precise measurements and that requires a significant amount of time. It appears that the 1/f noise components interfere with the measurement and increase the measurement errors. It has been demonstrated that flat field uniformity (see figures 6a, 6b) is much better than dispersion in gain measurements indicating that an average gain estimator is a better approximation of the pixel gain than the gain derived from the per pixel gain test.

I. Unit Cell Sensitivity

NISP requirements do not specify unit cell sensitivity however this parameter is helpful in comparing test results between different labs and monitoring the overall performance and manufacturing trends. Unit cell sensitivity is derived from the gain calibration and is listed in Table 4 for the PR3 detectors. We note that the Euclid detectors have a typical unit cell sensitivity approaching 5μV/e, a significant increase when compared with the 3.5μV/e for the older versions of the H2RG.

J. Science pixels

The NISP science pixels have to simultaneously meet four performance specifications: QE, spectroscopy noise, photometry noise and linearity. Masks derived from individual tests are combined to determine the final population of science pixels. A flight candidate SCA has to have at least 95% of all pixels meeting the four specifications. All subsequent parametric evaluation of the detector performance is based on this population of science pixels.

K. Thermal sensitivity

The stability of the NISP thermal system requires that the SCS parameters are unaffected by small temperature variations. The SCA thermal instability is specified as ±0.004K over 560s while the SCE instability is ±0.1K.

The impact of temperature instability on the SCS performance has been evaluated by a direct measurement of noise under emulated SCA and SCS temperature variations and by comparing the noise test results with those obtained under the condition of stable temperature conditions. For the duration of the noise test the FPA temperature was varied by ±0.004K over 560 seconds while the SCE temperature was maintained at 137K. Another test was performed where the SCE temperature was varied by ±0.1K over a 10 minute exposure while the FPA temperature was maintained at a constant 100K. Both tests were performed independently for SCA and SCE temperature variations. Results were indistinguishable within the measurement error when compared to the noise under stable temperature conditions. The SCA thermal sensitivity is determined by the readout electronics that is, by the multiplexer voltage followers. Thermal sensitivity is monitored by a direct measurement of the baseline shift as a function of temperature as illustrated in **Figure 14**. The typical SCA thermal coefficient is between 150 and 250 electron per degree Kelvin. It should be noted that the Euclid signal processing algorithms rely on reference pixels for the baseline correction that removes most of the thermal sensitivity. The reference correction reduces SCA thermal sensitivity from ~200e/K to less than 10e/K. Variation in the SCE temperature may have a significant impact on the SCS if the system configuration is not well adjusted. In properly adjusted systems, the SCE thermal coefficient is equivalent to approximately 10 electrons per Kelvin – see figure 15. Essentially the thermal sensitivity analysis serves as a monitoring tool for the quality of the configuration optimization.

Table 4 Summary of the thermal sensitivity for four Euclid detectors

Detector	Thermal Sensitivity [e/K]			SCE Thermal Sensitivity [e/K]	
	Image pixels	Reference pixels	Reference corrected	Uncorrected	Reference corrected
17243	-207.0	-200.7	-6.3	9.8	1.1
17192	-201.1	-198.4	-2.7	-8.5	-2.7
17178	-219.56	-219.6	0.04	-6.2	0.7
17246	-240.7	-229.6	-11.1	5.8	0.4

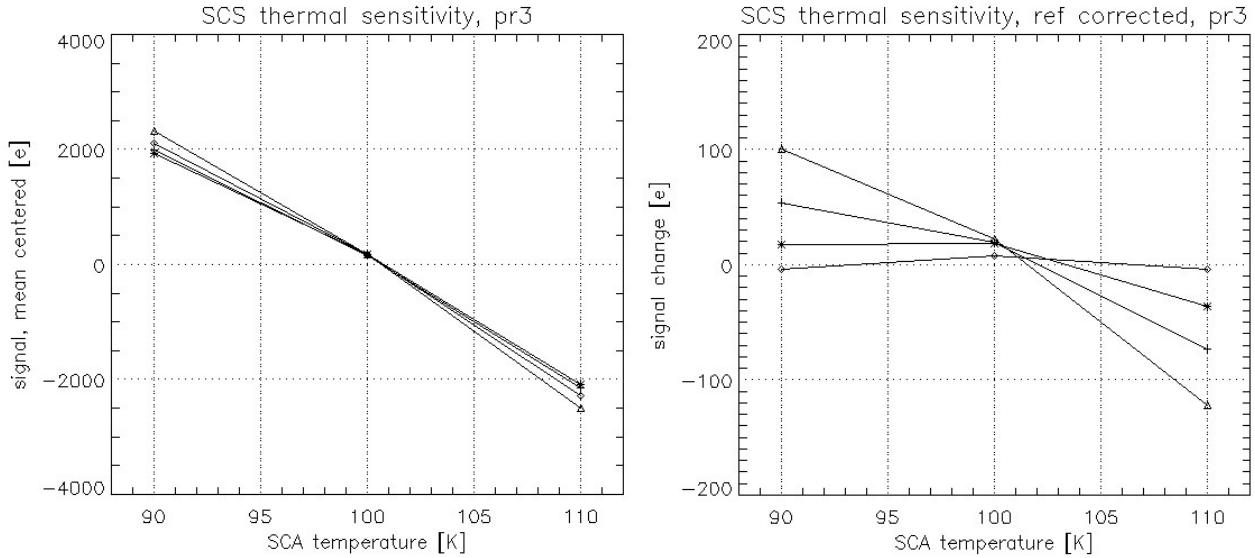

Figure 14. The SCA thermal sensitivity. Left : raw data; Right : after reference pixel correction

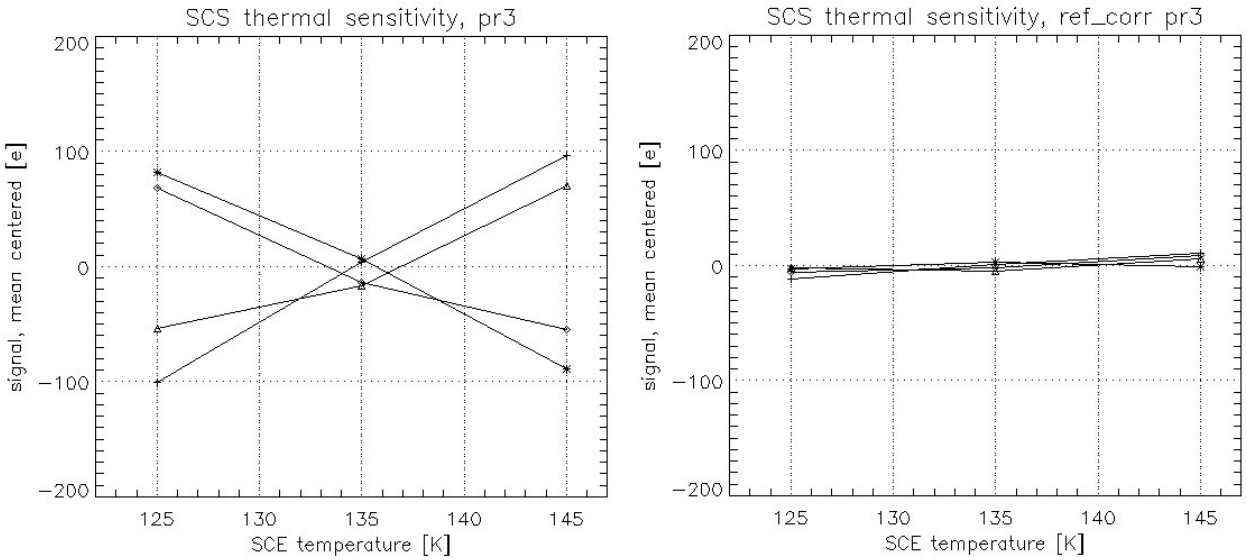

Figure 15 The SCS thermal sensitivity. Left: raw data; Right: after reference pixel correction

6. CONCLUSION

The Euclid project is an international collaboration of scientists and engineers involved with the United States and European Space Programs. It is an ambitious program with extremely high expectations of groundbreaking science data return. The Detector Characterization Laboratory of the NASA Goddard Space Flight Center in collaboration with the Jet Propulsion Laboratory, Teledyne Imaging Sensors and laboratories associated with the European Space Agency are working closely together to ensure that the infrared detector arrays that are installed in the NISP instrument are of the highest quality and as absolutely reliable as possible. To this end we have developed a custom testing program, evaluation and screening process to select the most suitable detector assemblies. Our test program is extremely comprehensive and capable of making the most sensitive measurements such as dark currents to less than 0.01 e/s or 1.6E-21 amps. In this paper we have given an overview of the test program we will be applying to the detectors, Sidecar ASICs and Cryo-Flex cables over the course of the next 12-24 months. In this time we expect to fully characterize 30 detector arrays, 20 Sidecar ASICs and re-test 20 detector/Sidecar subassemblies to yield 16 Flight modules for the Euclid NISP instrument. Thus far, the performance of the detectors and subsequently of the SCS units has been extremely good and all indications are that the TIS detectors and ASICs will be available and Flight worthy at the conclusion of this program.